Stability and bandgaps of layered perovskites for one- and two-photon water splitting

Castelli, Ivano Eligio; García Lastra, Juan Maria; Hüser, Falco Jonas; Thygesen, Kristian Sommer; Jacobsen, Karsten Wedel

Published in:
New Journal of Physics

Link to article, DOI:
10.1088/1367-2630/15/10/105026

Publication date:
2013

Document Version
Publisher's PDF, also known as Version of record

Stability and bandgaps of layered perovskites for one- and two-photon water splitting

2013 New J. Phys. 15 105026

(http://iopscience.iop.org/1367-2630/15/10/105026)

New Journal of Physics
The open access journal for physics

Stability and bandgaps of layered perovskites for one- and two-photon water splitting

Ivano E Castelli[1,3], **Juan María García-Lastra**[1,2], **Falco Hüser**[1], **Kristian S Thygesen**[1] **and Karsten W Jacobsen**[1]

[1] Center for Atomic-Scale Materials Design, Department of Physics, Technical University of Denmark, DK-2800 Kongens Lyngby, Denmark
[2] Nano-Bio Spectroscopy Group and ETSF Scientific Development Center, University of the Basque Country UPV/EHU, Avenida de Tolosa 72, E-20018 San Sebastian, Spain
E-mail: ivca@fysik.dtu.dk

New Journal of Physics **15** (2013) 105026 (14pp)
Received 11 June 2013
Published 28 October 2013
Online at http://www.njp.org/
doi:10.1088/1367-2630/15/10/105026

Abstract. Direct production of hydrogen from water and sunlight requires stable and abundantly available semiconductors with well positioned band edges relative to the water red-ox potentials. We have used density functional theory (DFT) calculations to investigate 300 oxides and oxynitrides in the Ruddlesden–Popper phase of the layered perovskite structure. Based on screening criteria for the stability, bandgaps and band edge positions, we suggest 20 new materials for the light harvesting photo-electrode of a one-photon water splitting device and 5 anode materials for a two-photon device with silicon as photo-cathode. In addition, we explore a simple rule relating the bandgap of the perovskite to the number of octahedra in the layered structure and the B-metal ion. Finally, the quality of the GLLB-SC potential used to obtain the bandgaps, including the derivative discontinuity, is validated against G_0W_0@LDA gaps for 20 previously identified oxides and oxynitrides in the cubic perovskite structure.

[3] Author to whom any correspondence should be addressed

Contents

1. Introduction

The direct conversion of solar light into chemical fuels through electrochemical reactions represents a clean, sustainable and potentially cheap alternative to fossil fuels. The simplest reaction of this kind is the water splitting (WS) reaction in which water is split into hydrogen and oxygen. In the most basic photo-electrochemical device, each photon is harvested by a single semiconductor and the created electron–hole pair is used to evolve hydrogen and oxygen. The maximum efficiency of such a one-photon device is only around 7% when overpotential of the reactions and losses are accounted for [1]. Significantly higher energy conversion efficiencies of up to 27% [2] can be achieved using a combination of two or more semiconductors with appropriately aligned band edges.

First attempts of photocatalytic WS were made in the 1970s using TiO_2 as the light harvesting and hydrogen evolving material [3]. Due to the large bandgap of TiO_2 and its poor catalytic properties the devices had extremely low efficiencies. Since then several materials have been proposed as light harvesting photo-electrodes for WS both in the UV and in the visible range [4]. Still, the efficiencies of the WS devices are significantly lower than the alternative combination of electrolysis driven by standard photovoltaic cells.

The search for new materials can be guided by *ab initio* quantum mechanical calculations, avoiding expensive 'trial and error' experimental processes. Recently, high-throughput materials design of stable binary and ternary alloys [5], carbon capture and storage [6], batteries [7], photovoltaic [8, 9] and WS materials [2, 10] have been reported. A number of databases have been also implemented to store and to analyze the huge amount of computed data generated. Some examples are the Materials Project database[4], the AFLOWLIB consortium [5] and the Computational Materials Repository[5].

In previous studies [2, 10], we have investigated the cubic perovskite structure and proposed 20 materials for the one-photon WS process and 12 others for the anode in a two-photon device with a Si cathode. Several of those were unknown in the WS community, but some of them have been already successfully tested. In particular the oxynitrides, like $BaTaO_2N$, $SrTaO_2N$, $CaTaO_2N$, $LaTiO_2N$ and $LaTaON_2$, gives good results in term of oxygen and/or hydrogen evolution in presence of sacrificial agents [11].

[4] Materials Project—A Materials Genome Approach (http://materialsproject.org/).
[5] Computational Materials Repository (documentation: https://wiki.fysik.dtu.dk/cmr/ and database: https://cmr.fysik.dtu.dk/).

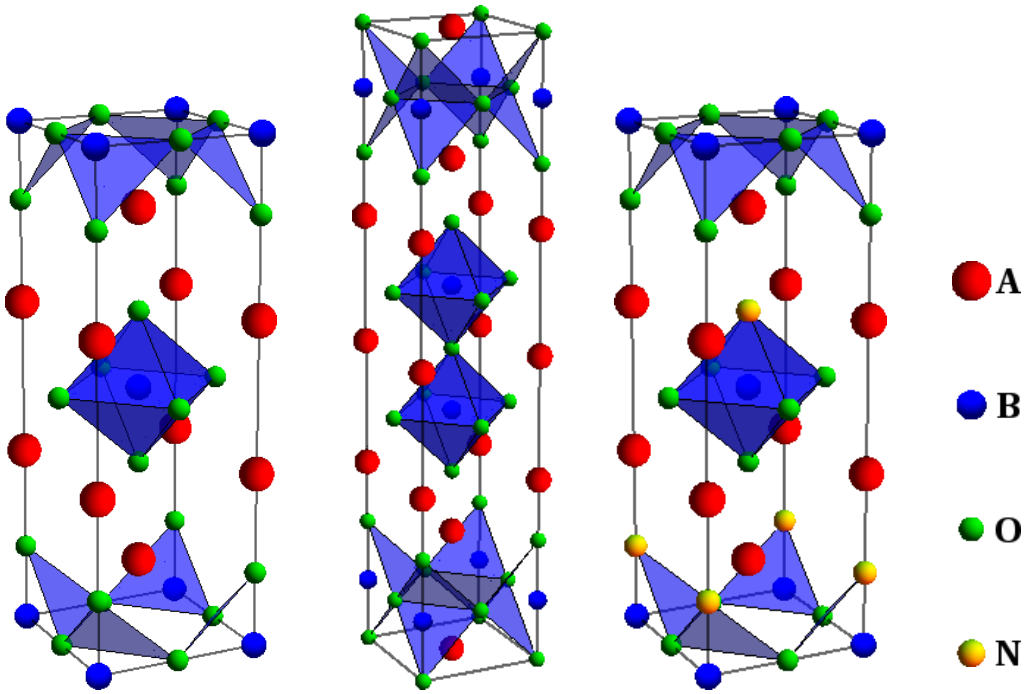

(a) A_2BO_4 (b) $A_3B_2O_7$ (c) A_2BO_3N

Figure 1. Crystal structure of the Ruddlesden–Popper phase with $n = 1$ (a) and $n = 2$ (b). Panel (c) shows the $n = 1$ structure when one oxygen is replaced by nitrogen. (a) A_2BO_4, (b) $A_3B_2O_7$ and (c) A_2BO_3N.

The perovskite is a very versatile structure with materials exhibiting a large variety of properties and applications [12]. In addition to the standard cubic and low-symmetry perovskites, two cubic perovskites with general formula ABO_3 can be combined together in the so-called double perovskite [13]. The double perovskite structure was recently explored with the focus of finding new materials for WS and engineering of the bandgap by combining two perovskites with different electronic properties [14, 15].

In the present work, we investigate the layered perovskite structure. A layered perovskite is composed of two-dimensional (2D) slabs of ABO_3 cubic perovskite separated by a motif of metal atoms. There are several phases of layered perovskites which differ in the thickness and the relative displacement of the cubic perovskite slabs and in the motifs. The phase studied here is the Ruddlesden–Popper with general formula $A_{n+1}B_nO_{3n+1}$, where $n = 1, \ldots, \infty$ is the number of BO_6 octahedra forming the 2D slabs and the upper limit for n correspond to the cubic phase. Figure 1 shows the structures under investigation: we consider the cases of $n = 1$ and $n = 2$ (A_2BO_4 and $A_3B_2O_7$, respectively) and one oxygen replacement in favor of nitrogen in the case of $n = 1$ (A_2BO_3N).[6] There are several distinct oxygen sites that can be replaced by nitrogen. To avoid large distortions in the octahedron, we replace the oxygen between the A- and B-atoms leaving the xy-plane of the octahedron unchanged. This unit cell does not allow

[6] The phases with $n = 1$ and 2 permit us to investigate the layered perovskite structures at a reasonable computational cost. The $n = 3$ structure is described by a 34 atoms unit cell, which is too demanding for a screening project.

to investigate possible symmetry lowering in the structure (i.e. octahedra tilting and Jahn–Teller distortions). In order to do that a larger unit cell is required, which would increase dramatically computational time, making the screening unaffordable. In any case we should remark that the use of a cubic symmetry is well justified since this symmetry lowering usually disappears at high temperatures. Indeed in many cases perovskites recover a cubic-like symmetry at room temperature [16, 17].

2. Method

In the one-photon WS device, one material is responsible for the evolution of both oxygen and hydrogen. First a photon is harvested creating an electron–hole pair. Next, the electron and hole reach two different points on the surface where the evolution of O_2 and H_2 takes place. Any material that should function as photo-electrode for WS should meet a number of criteria: (i) chemical and structural stability; (ii) a bandgap in the visible range; (iii) well positioned band edges with respect to the red-ox levels of water; and (iv) high mobility for electrons and holes. In addition, low cost and non-toxicity are required. Here we focus on the criteria (i)–(iii).

The stability of a material is evaluated with respect to around 2000 reference systems. The reference systems constitute stable phases of the possible materials into which the considered layered perovskite can be decomposed, and are taken from the experimental ICSD database[7] and the Materials Project database (see footnote 4). A material is considered stable only if the energy difference between the layered perovskite phase and the most stable alternative combination of reference systems is below 0.2 eV atom^{-1}. We use this finite threshold energy to avoid the exclusion of potential candidates due to inaccuracies in the calculations [18] and to take into account metastability of the investigated structure. Each combination is fully relaxed using the revised Perdew–Burke–Ernzerhof (RPBE) functional [19] implemented in the density functional theory (DFT)-GPAW code [20, 21].

As an example, the stability of the Ba_2TaO_3N compound is given by

$$\Delta E = \mathrm{Ba_2\,TaO_3N} - \min_{c_i}\Big\{c_1\mathrm{Ba_2} + c_2\,\mathrm{Ta_2} + c_3\mathrm{BaO} + c_4\mathrm{BaO_2} + c_5\mathrm{Ta_2O_5} + c_6\mathrm{BaN_6} + c_7\,\mathrm{Ta_3N_5} + c_8\mathrm{Ba_2\,TaN_3} + c_9\mathrm{BaTaO_2N} + c_{10}\mathrm{N_2} + c_{11}\mathrm{O}\Big\}, \quad (1)$$

where c_i are positive and sum up to assure the correct stoichiometry of the A_2BO_3N layered structure and the chemical formulae indicate the DFT total energies of the references. All the references are in their solid state phase except for N_2 and O which are in the gas phase. Note that the energy of oxygen is calculated from H_2 and H_2O due to the well known problems associated with the DFT description of the O_2 triplet ground state.

We note that the present stability analysis does not include corrosion of the materials. Extended stability analysis including this effect were recently found to be of some importance [22, 23]. However, we leave this for a future study.

It is well known that the Kohn–Sham eigenvalues from DFT systematically underestimate bandgaps of extended semiconductors due to the approximate nature of the exchange-correlation functionals and the missing derivative discontinuity [24]. On the other hand, many-body methods like the GW approximation give better bandgaps, but are computationally too expensive to be used in a screening project of several hundred materials. Here, we used the Gritsenko, van Leeuwen, van Lenthe and Baerends potential (GLLB) improved for solids (-SC)

[7] ICSDWeb (www.fiz-karlsruhe.de/icsd_web.html).

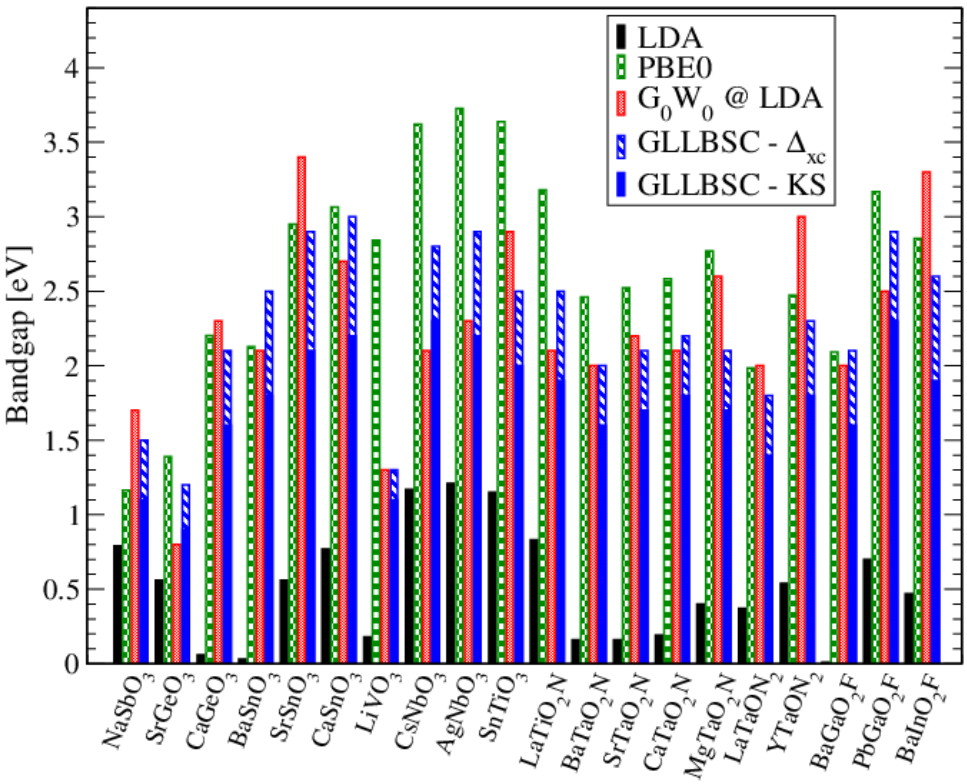

Figure 2. The bandgaps of the 20 identified candidates for one-photon WS calculated with the GLLB-SC potential (in blue) G_0W_0@LDA (in red), LDA (in black) and PBE0 (in green). The GLLB-SC bandgaps are obtained adding the derivative discontinuity (Δ_{xc}, in dashed blue) to the Kohn–Sham bandgap (KS, in solid blue). The discontinuities are usually proportional to the KS bandgaps. The agreement between the GLLB-SC potential and G_0W_0 is very good.

potential [25, 26], which includes an explicit estimation of the derivative discontinuity. In a previous work [10], the GLLB-SC bandgaps of around 40 metal oxides were compared to experiments. On average the GLLB-SC bandgaps were found to lie within 0.5 eV of the experimental gaps.

Figure 2 shows the bandgaps of the 20 earlier identified cubic perovskites for one-photon WS [2] here calculated using different methods and xc-functionals. Standard DFT functionals, like local density approximation (LDA) and PBE (not shown in the figure), seriously underestimate the bandgap, while the hybrid PBE0 tends to overestimate the gaps. We have performed G_0W_0 calculations using a recent implementation in the GPAW code [27]. In these calculations the G_0W_0 self-energy is evaluated using LDA energies and wave functions and the frequency dependence of the dielectric function is fitted to a plasmon pole model. We use a 150 eV plane wave cut off for the representation of the dielectric matrix and include empty bands up to the same energy cut off. A $7 \times 7 \times 7$ k-point mesh is used for both DFT and G_0W_0 calculations[8]. The GLLB-SC and G_0W_0 bandgaps are quite similar with a mean

[8] Convergence with respect to k points, plane wave cutoff and bands as well as validity of the plasmon pole approximation have been carefully tested for one of the structures. With the chosen parameters, we expect GW bandgaps to be converged within around 0.1 eV for all materials.

absolute difference of 0.3 eV. This is consistent with the results of a similar comparison made for a set of ten well characterized simple semiconductors and insulators [27]. Based on this we conclude that the bandgaps obtained with the GLLB-SC are sufficiently accurate for the purpose of materials screening.

In addition to the bandgap, the position of the conduction and valence band edges with respect to the water red-ox levels is crucial: the energy of electrons at the surface should be above the hydrogen evolution potential and the energy of holes must be below the oxygen evolution level. It is not trivial to calculate the band edge positions at a semiconductor–water interface from first principles. Although some methods have been proposed [28, 29], they are computationally rather demanding and not suited for screening studies. Instead we obtain the position of the band edges simply using an empirical equation [30, 31] that gives the center of the bandgap in terms of the geometrical average of the electronegativities in the Mulliken scale of the pure chemical elements, χ_M, forming the compound. The band edge positions are then calculated by adding and subtracting half of the bandgap, E_{gap}. In formula, for the A_2BO_4 layered perovskite:

$$E_{VB,\,CB} = E_0 + (\chi_A^2 \chi_B \chi_O^4)^{1/7} \pm E_{gap}/2\,, \tag{2}$$

where E_0 is the difference between the normal hydrogen electrode (NHE) and the vacuum ($E_0 = -4.5$ eV). More details about the method and its validation are available in [2, 10].

It has been recently shown for the cubic perovskite structure [32], that the search for new materials can be guided using chemical-based rules. The three chemical rules used here are:

- *Valence balance rule*: in a realistic material, the sum of the possible oxidation states of its elements must be zero.
- *Even–odd electrons rule*: the number of electrons per unit cell should be an even number. A material with an odd number of electrons has partially occupied bands at the Fermi level and is thus a metal. There are some exceptions to this rule, but they correspond to magnetic and/or strongly correlated materials which require more advanced theoretical descriptions than the one used here.
- *Ionic radii of the atoms*: the metals that can occupy the A- and B-ion position in the perovskite depend on the ionic radii of the neutral atoms. Usually alkali and alkaline earth metals occupy the A-ion side, and post-transition metals the B-ion position [12]. We implement this rule by having separate allowed chemical elements for the A- and B-sites[9].

The use of these rules drastically reduce the number of calculations from around 8000 to 300 different materials.

The screening parameters for the one-photon WS device are summarized in table 1. In addition to stability and a bandgap in the visible range, the band edges should straddle the red-ox levels of water plus the required overpotentials (0.1 eV for hydrogen and 0.4 eV for oxygen [33]).

The ideal efficiency of the one-photon device can be up to 7% [1]. Higher efficiencies can be achieved using a two-photon, or tandem, device, consisting of two semiconductors forming a pn-junction. Electrons generated in the cathode move to the surface and evolve hydrogen

[9] The metals used in the A-ion position are: Li, Na, Mg, K, Ca, Ga, Ge, Rb, Sr, Y, Ag, Cd, In, Sn, Cs, Ba, La, Tl and Pb. The B-metals are Al, Sc, Ti, V, Cr, Mn, Fe, Co, Ni, Cu, Zn, Ga, Ge, Zr, Nb, Mo, Ru, Rh, Pd, In, Sn, Sb, Te, Hf, Ta, W, Re, Os, Ir, Pt and Bi.

Table 1. Screening parameters (in eV) used for the one- and two-photon WS devices. The red-ox levels of water with respect to the NHE are 0 and 1.23 eV for the hydrogen and oxygen evolution, respectively. The criterion for the position of the band edges include also the overpotentials for hydrogen (0.1 eV) and for oxygen (0.4 eV) [33]. Silicon is used as cathode in the two-photon WS device ($VB^{Si}_{edge} = 0.86$ eV).

Criterion	One-photon WS	Two-photon WS
Stability (ΔE)	0.2 eV atom^{-1}	0.2 eV atoms^{-1}
Bandgap (E_{gap})	$1.7 \leqslant E_{gap} \leqslant 3$	$1.3 \leqslant E_{gap} \leqslant 3$
Band edges	$VB_{edge} > 1.6$	$VB^{anode}_{edge} > 1.6$
(VB_{edge}, CB_{edge})	$CB_{edge} < -0.1$	$CB^{cathode}_{edge} < -0.1$
		$CB^{anode}_{edge} < VB^{cathode}_{edge}$

while the holes move toward the pn-junction and recombine with electrons from the anode. Similarly, the holes generated in the anode move toward the surface and evolve oxygen. Thus it takes two photons to generate one H_2. The efficiency of the device depends strongly on the relative sizes of the bandgaps of the two materials. Assuming ideal band edge line up, the best performance (around 25%) is obtained by combining two materials with bandgaps of 1.1 eV and 1.7, respectively [2]. The sum of the two bandgaps should not be smaller than 2.8 eV: 1.23 eV is the energy required per electron to split water and approximately 0.5 eV is required to account for the overpotentials of the oxidation and reduction reactions. In addition, the relevant quasi-Fermi levels are located ≈ 0.25 eV below (above) the conduction (valence) bands[10]. Finally, the quasi-Fermi level corresponding to the conduction band of the cathode should be at least 0.1 eV above the quasi-Fermi level corresponding to the valence band of the anode to ensure efficient charge recombination at the interface. As it turns out, silicon is an ideal photo-cathode for WS since it has a bandgap of 1.1 eV well positioned with respect to the reduction potential of hydrogen and because of the mature fabrication technology. A more detailed explanation of the two-photon device is available in [2]. In the case of two-photon devices we therefore limit our search to photo-anode materials assuming a silicon cathode and use the screening criteria summarized in table 1.

3. Trends in stability and bandgaps

The simplest layered perovskite is the Ruddlesden–Popper phase. The two phases studied here have the general formula A_2BO_4 and $A_3B_2O_7$. The former is composed of slabs of cubic perovskite ABO_3 offset by a translation of $(1/2, 1/2)$ with respect to each other, terminated by oxygens to complete the octahedra, and separated by a layer of A metal atoms. In the latter structure each slab of perovskite is formed by two octahedra BO_6 units. The unit cells

[10] The quasi-Fermi level describes the population electrons and holes in a semiconductor when their populations are not in equilibrium, for example when the semiconductor is under illumination. When an electron–hole pair is created, the density of both electrons and holes are above their equilibrium values and the populations of the carriers cannot be described by a single Fermi level. One of the consequences of the quasi-Fermi levels is that the effective energy of the electrons and holes does not correspond anymore to the conduction and valence band but the quasi-Fermi levels have to be considered.

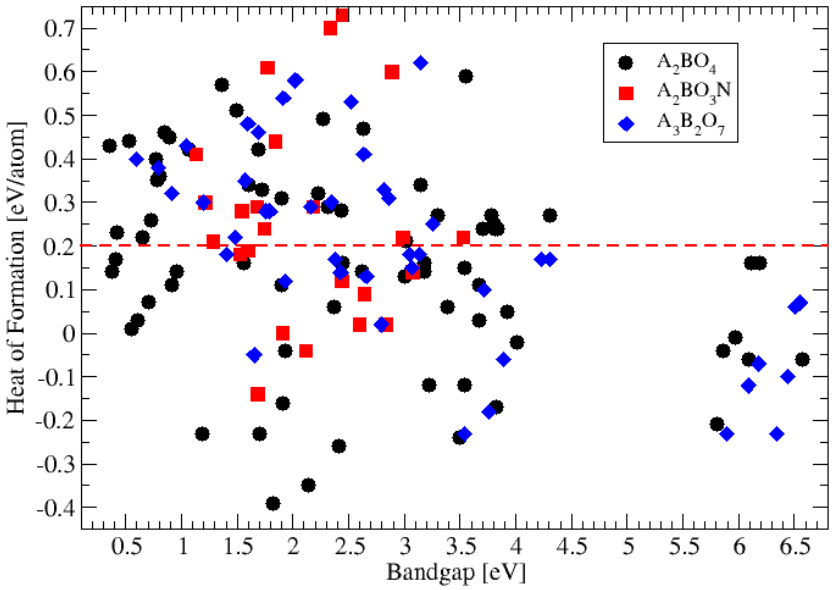

Figure 3. Calculated heat of formation plotted versus bandgap for the A_2BO_4 (black circles), A_2BO_3N (red squares) and $A_3B_2O_7$ (blue diamonds). The oxides show high stability and a wide range of bandgaps. The oxynitrides are overall less stable and have smaller bandgaps than the oxides.

of the two phases contain 14 and 24 atoms, respectively. The A-ion position is generally occupied by an alkali or alkali-earth metal, and the B-ion by a transition or post-transition metal. Materials of the form A_2BO_3N, in which an oxygen atom has been replaced by nitrogen, have been considered. In general, oxides tend to have valence band edges that are somewhat deep compared to the oxidation potential of water. Nitrogen is slightly less electronegative compared to oxygen and the valence bands of the oxynitrides are consequently shifted up compared to the oxides [34]. The smaller electronegativity of nitrogen leads also to a reduction in the size of the bandgaps. In addition, a nitrogen replacement breaks the symmetry of the cubic perovskite and creates an excess of charge in one of the corners of the octahedron. This leads to a reduction in the stability of the obtained materials, as shown in figure 3.

Figure 3 shows the calculated heat of formation for the A_2BO_4, A_2BO_3N and $A_3B_2O_7$ perovskites plotted against the GLLB-SC bandgap. The bandgaps of both types of oxides range from 0 to above 6 eV. The oxides are in general highly stable especially the materials with larger bandgaps. As expected, the oxynitrides are less stable and show smaller gaps. Despite of this, around 8 oxynitrides are found to fulfill the criteria on bandgap and stability for the one-photon WS device. A further nitrogen replacement is likely to lower the bandgaps and reduce the stability even further [2], and therefore has not been investigated here.

All the bandgaps of the stable A_2BO_4 layered perovskites are plotted in figure 4. There is some degree of correlation between the chemical elements and the size of the bandgaps. First of all it can be seen that the gap is mainly determined by the B-ion while the A-ion has less influence. Hf and Zr in the B-ion position generate large bandgap insulators with gaps above 6 eV. Ti, Ge and Sn lead to structures with gaps above 3 eV while W and Zn produce structures with gaps around 2 eV.

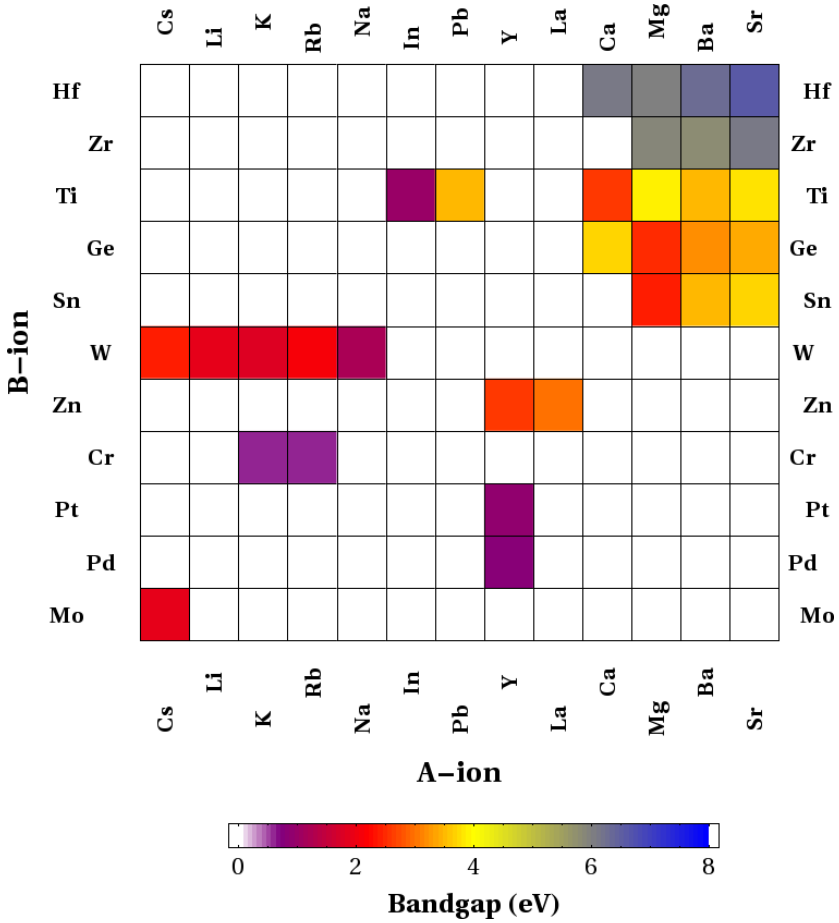

Figure 4. Bandgaps of the stable compounds in the A_2BO_4 structure. The gaps range from 0 to more than 6 eV. The chemical elements are sorted for similarity so that atoms that generate layered perovskites with similar bandgaps are close together.

Most of the oxides investigated have valence bands formed by the 2p levels of the O^{2-} ions. Since the nature of the bonds in these materials is highly ionic, this implies that the top of the valence band is roughly the same for all the oxides[11]. The conduction bands are mainly composed of the lowest unoccupied molecular orbitals (LUMO) of the A and B metal ions. This means that the size of the bandgap should correlate with the lowest lying LUMO level of the A and B cations. The relevant LUMO level is, however, not that of the cations in vacuum, but rather a cation sitting in the electrostatic field from the rest of the lattice, V_R. To analyze this, we follow an Ewald–Evjen scheme, assuming that all the ions keep their nominal charges. This scheme is described elsewhere in the literature [35].

Table 2 shows how the LUMO energies change drastically passing from the free cations to the cations under the effect of V_R. V_R destabilizes much more the energies of the B-site ions than

[11] There are some exceptions to these rule, e.g. those compounds that contain carbon group ions with valence 2+ (Ge^{2+}, Sn^{2+} and Pb^{2+}), in which the valence band is a mix between the 2p levels of the O^{2-} ions and the s levels of the carbon group ion.

Table 2. LUMO energies (in eV) of several B^{4+} ions in vacuum and in the presence of the crystal electrostatic field V_R, respectively. V_R is calculated for $ASnO_4$ and $CaBO_4$ for the A^{2+} and B^{4+} ions, respectively, (similar results are obtained for other lattices). The LUMO energies of the A^{2+} ions in vacuum and under the effect of V_R are for Ca^{2+} (s): −14.65 and −0.58; for Sr^{2+} (s): −13.58 and −1.02; and for Cd^{2+} (s): −20.35 and −4.91. The bandgaps of the compounds containing these ions are also shown for comparison.

			Bandgap		
B-ion	In vacuum	Including V_R	Ca_2BO_4	Sr_2BO_4	Cd_2BO_4
Ti^{4+} (d)	−56.13	−3.35	4.01	3.82	0.78
Zr^{4+} (d)	−42.30	−1.24	6.19	6.09	1.90
Hf^{4+} (d)	−39.90	−1.10	6.11	6.57	1.60
Ge^{4+} (s)	−52.28	−3.64	3.67	3.39	0.36
Sn^{4+} (s)	−45.45	−3.82	3.70	3.67	0.54

the ones of the A-site ions. This is due to the short distance between the O^{2-} and A ions (usually in a range from 1.9 to 2.3 Å) in comparison with the B–O^{2-} distances (in a range from 2.5 to 3.0 Å). The table shows the correlation between the lowest LUMO energy from A and B (under the effect of V_R) ions and the bandgap for the particular case of $(A^{2+})_2B^{4+}(O^{2-})_4$ perovskites. The LUMO of the B^{4+} ions is more stable than the LUMO of the A^{2+} ions when the A position is occupied by an alkaline-earth ion (in the table only the results for Ca^{2+} and Sr^{2+} are shown, but similar features are observed for Mg^{2+} and Ba^{2+}). Thus, in these cases the bandgap is correlated with the LUMO of the B ion. This explains why Zr^{4+} and Hf^{4+} compounds have similar gaps, whereas Ti^{4+} shows a smaller gap. This could be understood even just by looking at the energies of the ions in vacuum, since the d-levels of Ti^{4+} are much deeper in energy that those of Zr^{4+} and Hf^{4+}. This difference is strongly reduced when V_R is considered due to the smaller ionic radius of Ti^{4+} (10 pm smaller than Zr^{4+} or Hf^{4+} ionic radii [36]), which has O^{2-} ions closer. In the case of the carbon group (Ge^{4+} and Sn^{4+}), their compounds have similar bandgaps due to a compensation of effects: Ge^{4+} s level in vacuum is lower in energy than Sn^{4+} s level (by ≈ 7 eV), but Ge^{4+} ionic radii is 16 pm smaller than that of Sn^{4+}.

When Cd^{2+} occupies the A site, its LUMO (the s level) is more stable than the LUMO of B^{4+} ions, contrary to the case of an alkaline-earth on A position. This leads to compounds with a conduction band dominated by the Cd^{2+} s level and consequently to a small bandgap. A similar investigation has been performed also for the $A_3B_2O_7$ layered perovskites with similar results. Since nitrogen has an electronegativity very close to the one of oxygen, we expect that these results are still valid for the oxynitrides. The main difference will be that the valence band is formed by an hybridization of the oxygen and nitrogen 2p orbitals.

A couple of A- and B-ions can be used for both the A_2BO_4 and the $A_3B_2O_7$ perovskites. For these cases, we have investigated the changes in the size of the bandgaps depending on the number of octahedra forming the 2D slab. There is a weak trend that correlates the bandgaps to the B-ions: when the B-ion position is occupied by a p-metal (e.g. Ge and Sn) the gaps are generally reduced when the slab thickness is increased, while for d-metals (e.g. Ti, Zr and Hf), the gaps seem to increase with slab thickness. In average, for the p-metals the bandgaps are reduced by 0.6 eV from the $n = 1$ to $n = 2$ structures and by 0.4 eV from the $n = 1$ to $n = \infty$

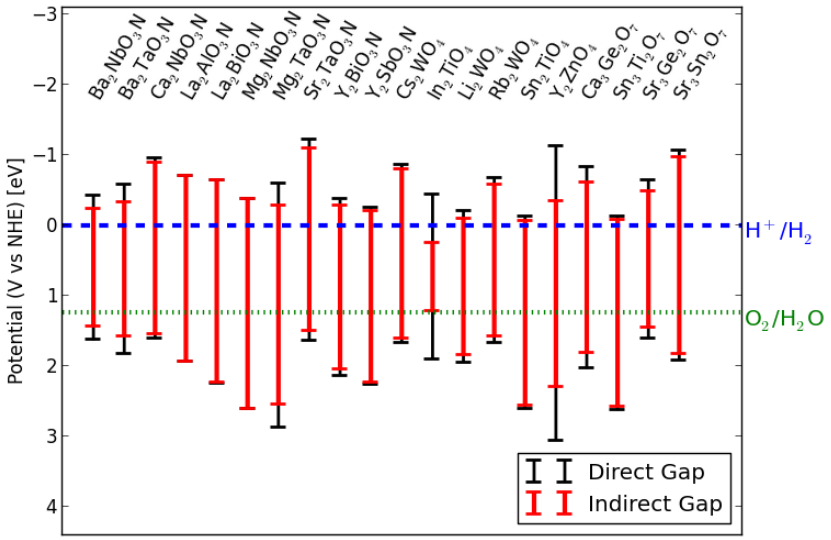

Figure 5. The identified candidates in the Ruddlesden–Popper phases for one-photon WS. The figure shows the red-ox levels of water and the calculated band edges for the indirect (red) and direct (black) bandgaps.

structures. For the d-metals the bandgaps are reduced by 0.03 and 0.2 eV, respectively. There are some exceptions to this trend, like $Sr_{n+1}Ti_nO_{3n+1}$. Lee *et al* [37] have recently shown that bandgaps of the $Sr_{n+1}Ti_nO_{3n+1}$ Ruddlesden–Popper phase is reduced with an increase of the thickness and we have seen the same effect. In general, these trends could be used to tune the bandgap by increasing or reducing the number of octahedra within the layers.

4. Candidates for water splitting

The screening criteria of table 1 have been applied to the calculated structures. Out of the 300 investigated materials 20 fulfill the criteria for one-photon WS, see figure 5. Ba_2TaO_3N and $Sr_3Sn_2O_7$ are known to exist experimentally in the layered perovskite structure. Ba_2TaO_3N has also recently been proposed as a WS material by Wu *et al* [38] who used a computational screening procedure similar to the one proposed here. Y_2BiO_3N and the other $A_3B_2O_7$ compounds are already known in other stoichiometries and most of the A_2BO_4 materials and Sr_2TaO_3N have been synthesized in other crystal structures with the same stoichiometry as the layered perovskite. It might not be an issue that some compounds are known in another crystal structure. In fact, layered perovskites can often be grown epitaxially even if they are not globally stable. Eight of the identified perovskites have not been investigated experimentally to our knowledge. In particular, the oxynitrides are interesting candidates for WS. In fact, the cubic perovskites ABO_2N with A = Ba, Sr and Ca, and B = Ta and Nb are known to evolve hydrogen and/or oxygen in the presence of a sacrificial agent [11, 39]. We expect that the layered perovskites containing these elements conserve the good properties in terms of activity already present in the cubic phase.

For the two-photon device with a silicon cathode, our screening identifies five layered perovskites as candidates for the anode material. All five are experimentally known in other structures/stoichiometry, but none of them has been used so far as photocatalyst.

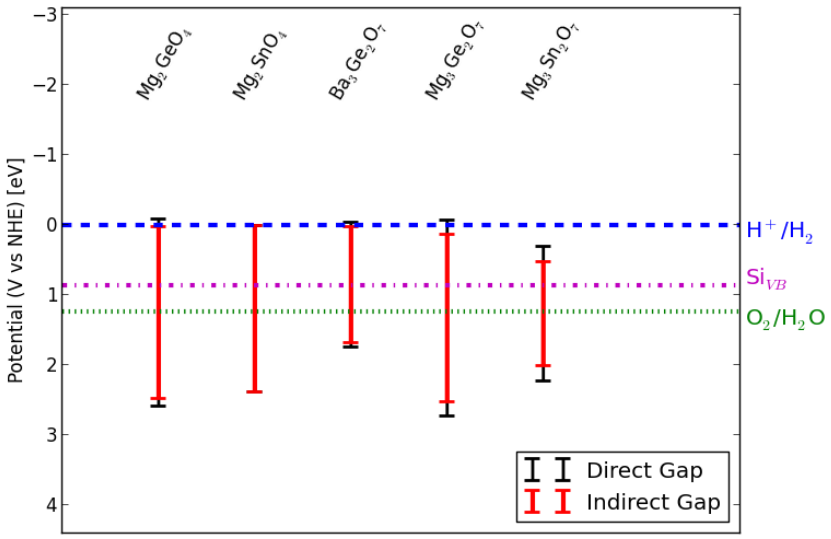

Figure 6. The identified candidates in the Ruddlesden–Popper phases for two-photon WS device. The figure shows the red-ox levels of water and the valence band of silicon. The calculated band edges for the indirect (red) and direct (black) bandgaps are drawn.

5. Conclusions

With the aim of identifying stable and abundantly available semiconductors for light harvesting photo-electrodes for WS, we have screened 300 oxides and oxynitrides in the layered perovskite structure with stoichiometry A_2BO_4, $A_3B_2O_7$ and A_2BO_3N. The stability and bandgaps were calculated using DFT and the band edge alignment relative to the water red-ox potentials was estimated using an empirical formula. The accuracy of the calculated bandgaps, which were obtained with the GLLB-SC potential, was validated by comparing with state of the art G_0W_0 calculations for 20 oxides in the cubic perovskite structure.

We have identified 20 candidate materials for one-photon WS, and additional 5 materials for photo-anode in a two-photon device with a silicon cathode. A few of these materials are already experimentally known, but none of them have been used so far for photoelectrocatalysis.

The trends in stability and bandgap have been studied in some detail. We have found that the bandgap of the layered perovskites is mainly determined by the position of the most stable LUMO of the A- and B-ion. Furthermore, our results indicate that the bandgap can be tuned to some extent by varying the number of octahedra forming the layered structure. Specifically, for a d-metal (p-metal) at the B-ion position the effect is to increase (decrease) the gap with the number of octahedra within a layer.

Acknowledgments

The authors acknowledge support from the Catalysis for Sustainable Energy (CASE) initiative funded by the Danish Ministry of Science, Technology and Innovation and from the Center on Nanostructuring for the Efficient Energy Conversion (CNEEC) at Stanford University, an Energy Frontier Research Center founded by the US Department of Energy, Office of Science,

Office of Basic Energy Sciences under award number DE-SC0001060. JMGL acknowledges support from the Spanish Ministry of Economy and Competitiveness under project numbers FIS2009-07083, FIS2010-21282-C02-01 and FIS2012-30996 and through Ramon y Cajal grant number RYC-2011-07782.

References

[1] Weber M R and Dignam M J 1986 Splitting water with semiconducting photoelectrodes-efficiency considerations *Int. J. Hydrog. Energy* **11** 225–32
[2] Castelli I E, Landis D D, Thygesen K S, Dahl S, Chorkendorff Ib, Jaramillo T F and Jacobsen K W 2012 New cubic perovskites for one- and two-photon water splitting using the computational materials repository *Energy Environ. Sci.* **5** 9034–43
[3] Fujishima A and Honda K 1972 Electrochemical photolysis of water at a semiconductor electrode. *Nature* **238** 37–8
[4] Kudo A and Miseki Y 2009 Heterogeneous photocatalyst materials for water splitting. *Chem. Soc. Rev.* **38** 253–78
[5] Curtarolo S *et al* 2012 Aflow: an automatic framework for high-throughput materials discovery *Comput. Mater. Sci.* **58** 218–26
[6] Lin *et al* 2012 *In silico* screening of carbon-capture materials *Nature Mater.* **11** 633–41
[7] Ceder G, Chiang Y -M, Sadoway D R, Aydinol M K, Jang Y -I and Huang B 1998 Identification of cathode materials for lithium batteries guided by first-principles calculations *Nature* **392** 694
[8] Hachmann J, Olivares-Amaya R, Atahan-Evrenk S, Amador-Bedolla C, Sanchez-Carrera R S, Gold-Parker A, Vogt L, Brockway A M and Aspuru-Guzik A 2011 The Harvard clean energy project: large-scale computational screening and design of organic photovoltaics on the world community grid *J. Phys. Chem. Lett.* **2** 2241–51
[9] d'Avezac M, Luo J -W, Chanier T and Zunger A 2012 Genetic-algorithm discovery of a direct-gap and optically allowed superstructure from indirect-gap Si and Ge semiconductors *Phys. Rev. Lett.* **108** 027401
[10] Castelli I E, Olsen T, Datta S, Landis D D, Dahl S, Thygesen K S and Jacobsen K W 2012 Computational screening of perovskite metal oxides for optimal solar light capture *Energy Environ. Sci.* **5** 5814
[11] Yamasita D, Takata T, Hara M, Kondo J N and Domen K 2004 Recent progress of visible-light-driven heterogeneous photocatalysts for overall water splitting *Solid State Ion.* **172** 591–5
[12] Ishihara T 2009 *Perovskite Oxide for Solid Oxide Fuel Cells* (Berlin: Springer)
[13] Kobayashi K-I, Kimura T, Sawada H, Terakura K and Tokura Y 1998 Room-temperature magnetoresistance in an oxide material with an ordered double-perovskite structure *Nature* **395** 677–80
[14] Berger R F and Neaton J B 2012 Computational design of low-band-gap double perovskites *Phys. Rev.* B **86**
[15] Castelli I E, Thygesen K S and Jacobsen K W 2013 Bandgap engineering of double perovskites for one- and two-photon water splitting *MRS Online Proc. Libra.* **1523**
[16] Megaw H D 1945 Crystal structure of barium titanate *Nature* **155** 484–5
[17] Møller C K 1957 A phase transition in cæsium plumbochloride *Nature* **180** 981–2
[18] Honkala K, Hellman A, Remediakis I N, Logadottir A, Carlsson A, Dahl S, Christensen C H and Nørskov J K 2005 Ammonia synthesis from first-principles calculations *Science* **307** 555–8
[19] Hammer B, Hansen L B and Nørskov J K 1999 Improved adsorption energetics within density-functional theory using revised Perdew–Burke–Ernzerhof functionals *Phys. Rev.* B **59** 7413–21
[20] Mortensen J J, Hansen L B and Jacobsen K W 2005 Real-space grid implementation of the projector augmented wave method *Phys. Rev.* B **71** 35109
[21] Enkovaara J *et al* 2010 Electronic structure calculations with GPAW: a real-space implementation of the projector augmented-wave method *J. Phys.: Condens. Matter* **22** 253202
[22] Persson K A, Waldwick B, Lazic P and Ceder G 2012 Prediction of solid-aqueous equilibria: scheme to combine first-principles calculations of solids with experimental aqueous states *Phys. Rev.* B **85** 235438

[23] Castelli I E, Thygesen K S and Jacobsen K W 2013 Calculated Pourbaix diagrams of cubic perovskites for water splitting: a critical stability analysis *Top. Catalysis* accepted
[24] Godby R W, Schlüter M and Sham L J 1986 Accurate exchange-correlation potential for silicon and its discontinuity on addition of an electron *Phys. Rev. Lett.* **56** 2415–8
[25] Gritsenko O, van Leeuwen R, van Lenthe E and Jan Baerends E 1995 Self-consistent approximation to the Kohn–Sham exchange potential *Phys. Rev.* A **51** 1944
[26] Kuisma M, Ojanen J, Enkovaara J and Rantala T T 2010 Kohn–Sham potential with discontinuity for band gap materials *Phys. Rev.* B **82** 115106
[27] Hüser F, Olsen T and Thygesen K S 2013 Quasiparticle GW calculations for solids, molecules and two-dimensional materials *Phys. Rev.* B **87** 235132
[28] Wu Y, Chan M K Y and Ceder G 2011 Prediction of semiconductor band edge positions in aqueous environments from first principles *Phys. Rev.* B **83** 235301
[29] Georg Moses P and Van deWalle C G 2010 Band bowing and band alignment in ingan alloys *Appl. Phys. Lett.* **96** 021908
[30] Butler M A and Ginley D S 1978 Prediction of flatband potentials at semiconductor–electrolyte interfaces from atomic electronegativities *J. Electrochem. Soc.* **125** 228–32
[31] Xu Y and Schoonen M A A 2000 The absolute energy positions of conduction and valence bands of selected semiconducting minerals *Am. Mineral.* **85** 543–56
[32] Jain A, Castelli I E, Hautier G, Bailey D H and Jacobsen K W 2013 Performance of genetic algorithms in search for water splitting perovskites *J. Mater. Sci.* **48** 6519–34
[33] Trasatti S 1990 *Croat. Chem. Acta* **63** 313–29
[34] Aguiar R, Logvinovich D, Weidenkaff A, Rachel A, Reller A and Ebbinghaus S G 2008 The vast colour spectrum of ternary metal oxynitride pigments *Dyes Pigments* **76** 70–5
[35] Piken A G and van Gool W 1968 *Ford Tech. Report* SL 68-10
[36] Shannon R D 1976 Revised effective ionic radii and systematic studies of interatomic distances in halides and chalcogenides *Acta Crystallogr.* A **32** 751–67
[37] Lee C-H *et al* 2013 Effect of reduced dimensionality on the optical band gap of $SrTiO_3$ *Appl. Phys. Lett.* **102** 122901
[38] Wu Y, Lazic P, Hautier G, Persson K and Ceder G 2013 First principles high throughput screening of oxynitrides for water-splitting photocatalysts *Energy Environ. Sci.* **6** 157–68
[39] Siritanaratkul B, Maeda K, Hisatomi T and Domen K 2011 Synthesis and photocatalytic activity of perovskite niobium oxynitrides with wide visible-light absorption bands *ChemSusChem* **4** 74–8